Convectively Coupled Waves Propagating along an Equatorial ITCZ

JULIANA DIAS AND OLIVIER PAULUIS

New York University, New York, New York

(Manuscript received 1 December 2008, in final form 14 February 2009)

ABSTRACT

The dynamics of convectively coupled gravity waves traveling over a precipitating region are analyzed in an idealized model for the large-scale atmospheric circulation. The model is composed of a shallow water system coupled to an advection equation for moisture through the convection term, utilizing a quasi-equilibrium relaxation to moisture closure. Here the authors investigate the model in the strict quasi-equilibrium (SQE) of infinitely short relaxation time. This framework is applied to study the behavior of a disturbance propagating along a narrow precipitation band, similar to the intertropical convergence zone (ITCZ). For an ITCZ width on the order of the equatorial Rossby radius, Kelvin waves propagate at the moist gravity wave speed (about 15 m s^{-1}), whereas for a narrow ITCZ, the propagation speed is comparable to the dry gravity wave (about 50 m s^{-1}). It is also shown that a Kelvin wave propagating along a narrow precipitation region exhibits a meridional circulation that modulates the precipitation rate and affects the propagation speed of the wave.

1. Introduction

The propagation of tropical disturbances is strongly affected by the interactions among atmospheric circulation, moisture transport, and convection. These interactions are at the core of many atmospheric issues such as hurricanes, the Madden–Julian oscillation, and planetary circulation (Emanuel 1986; Madden and Julian 1971; Pauluis 2004). The present study focuses on the interaction between deep convection in the intertropical convergence zone (ITCZ) and equatorial waves and, in particular, on how the width of the ITCZ impacts the propagation speed and structure of equatorial Kelvin waves.

In the tropics, energy absorbed at the surface over the tropical oceans is transferred to the lower troposphere through evaporation and then transported to higher altitudes through convection and latent heat release. The ascending branch of the Hadley circulation corresponds to a region of low-level convergence, the ITCZ. The ITCZ is characterized by a region of increased convection, cloudiness, and precipitation; therefore, fluxes of heat, moisture, and momentum vary dramatically inside and outside the ITCZ and impact the tropical circulation.

A number of observational works have been undertaken to clarify the interaction between clouds and atmospheric disturbances. By means of wavenumber–frequency spectral analysis of satellite data, studies such as Wheeler and Kiladis (1999) obtained considerable success in quantifying the relationship between the dynamical structure of equatorial waves and moist convection. These convective propagating disturbances are called convectively coupled equatorial waves (CCEWs) because they present characteristics similar to the equatorially trapped shallow water modes found in Matsuno (1966); however, there are some important differences. Wheeler and Kiladis (1999) found that these modes propagate more slowly than they would in the absence of precipitation and that low-wavenumber Kelvin modes propagate faster than the corresponding high-wavenumber mode. In Straub and Kiladis (2002), evidence is shown of convective activity propagating along the mean axis of the eastern Pacific ITCZ with the spatial structure, propagation speed, and dispersion characteristics of the equatorially trapped Kelvin waves. It is also shown that the coupled Kelvin wave, unlike the traditional Kelvin wave, has a nonnegligible meridional component in regions of deep convection. Moreover, in Wheeler et al. (2000), convectively coupled Kelvin waves are shown to be weakly dispersive.

The theory for equatorial trapping of large-scale wavelike disturbances was discovered by Matsuno (1966), who

Corresponding author address: Juliana Dias, New York University, 251 Mercer St., New York, NY 10012.
E-mail: dias@cims.nyu.edu

DOI: 10.1175/2009JAS3020.1

derived a complete set of linear wave mode solutions of the shallow water equations on the equatorial β plane. Since then, shallow water analytical models have been extensively used to gain basic insight into the response of the tropical atmosphere to heating. For instance, Gill (1980) utilized a linear shallow water model forced by a stationary heat source concentrated in specific areas to study how equatorial propagating modes are affected by diabatic heating. Although these models provide relevant simulations of tropical anomalies, they have the limitation that the active role of tropical convection is not resolved.

The quasi-equilibrium (QE) theory is a convective closure that was originally proposed by Arakawa and Schubert (1974) and assumed that convective motions act to eliminate convective instability over an adjustment time scale of a few hours. Based on the time scale separation between the convective adjustment time and synoptic or planetary circulation, they find that the rate of change of convective instability, quantified in terms of the cloud work function, remains small in convectively active regions. Under similar assumptions, Emanuel et al. (1994) argue that the effect of convection on the large-scale circulation is to reduce the effective static stability of the atmosphere (or the equivalent depth) and therefore gravity waves must slow down. Moreover, based on studies such as Betts (1986) that suggest a convective adjustment time between 2 and 24 h, Emanuel et al. (1994) proposed the strict quasi-equilibrium (SQE) theory, in which the atmosphere is instantaneously relaxed toward a moist adiabatic profile in convective regions. This assumption greatly simplifies theoretical investigations of the interaction of convection and the planetary scale because it eliminates the need for a description of the behavior of individual clouds.

However, the original derivation of the SQE theory has an important limitation: the requirement of an atmosphere in which precipitation is active everywhere. In Frierson et al. (2004, hereafter FMP04), the QE framework is applied to the study of the interface between precipitating and nonprecipitating regions (the precipitation front), assuming SQE and in one space dimension. Utilizing a similar model, Pauluis et al. (2008) found stationary precipitation fronts in an idealized Walker circulation background flow, in both one and two dimensions. In Stechmann and Majda (2006), the precipitation front theory in one space dimension is extended to finite convective adjustment time; they show that for a small convective adjustment time their results are in agreement with the SQE theory.

The present work is an extension of FMP04 and Pauluis et al. (2008) for a particular version of the two-dimensional problem in which, assuming SQE, the behavior of large-scale waves propagating along a narrow precipitation band (the ITCZ) is investigated. The main advantage that the SQE framework offers in this case is the simplicity of analysis of the interaction between a precipitating region and propagating disturbances. However, the results have to be carefully interpreted because the applicability of the QE (and SQE) assumption is certainly incorrect at the scale of individual clouds. Nonetheless, the present approach can give insight into dealing with the roll of moisture in the tropics and, because general circulation models are frequently based on QE concepts, it can also be used to explain some of the behavior of these models.

The paper is organized as follows: In section 2, we present the model equations and review the main implications of the SQE assumption. This framework is then applied in section 3 to study the propagation of CCEWs along a precipitating band parallel to the equator. First, we obtain stationary solutions (i.e., the stationary precipitating band, associated with an idealized Hadley circulation). In this model, both the location and width of the ITCZ are controlled by imposing the surface temperature. We then derive the disturbance equations to investigate the behavior of perturbations. In section 4, the analytical and numerical results are presented, including the convectively coupled Kelvin and Rossby waves propagating on precipitating bands of distinct width and location. The effects of the ITCZ on both the meridional flow and the propagation speed of the CCEW, as well as the interaction between the coupled waves and the displacement of the precipitation front, are discussed in section 5. The main results are summarized in section 6, and the analytical and numerical solutions are described in the appendixes.

2. Model description

The model used here is based on a Galerkin truncation of the equations of motion into a finite set of vertical modes, equivalent to the quasi-equilibrium tropical circulation model (QTCM) from Neelin and Zeng (2000). There are a number of versions of models similar to the QTCM and in this paper we utilize the model from FMP04, in which a detailed derivation and discussion of its mathematical aspects is presented.

In the QTCM the barotropic and first baroclinic modes are retained; however, in the present work, for mathematical simplicity, we only consider the first baroclinic mode on the β plane, coupled to a vertically averaged moisture equation. The first baroclinic vertical structure (winds in the lower troposphere of equal magnitude and opposite signal to those in the upper troposphere) is a fairly good approximation in regions of

deep convection (Takayabu 1994) and has been used in several studies of the tropics. Moreover, because deep convection is known to play a key role in the interaction between water vapor and large-scale dynamics, the vertically averaged moisture is a reasonable approximation for the purposes of this work. The governing equations are

$$\partial_t u - \partial_x T - yv = -\kappa u, \tag{1a}$$

$$\partial_t v - \partial_y T + yu = -\kappa v, \tag{1b}$$

$$\partial_t T - \nabla \cdot \mathbf{u} = P - R, \quad \text{and} \tag{1c}$$

$$\partial_t q + \tilde{Q}\nabla \cdot \mathbf{u} = -P + E, \tag{1d}$$

where the main variables are the horizontal velocity $\mathbf{U} = \mathbf{u}(x, y, t)\Psi_u(z)$, the potential temperature $T = T(x, y, t)\Psi_T(z)$, the vertical velocity $W = w(x, y, t)\Psi_w(z)$, and the height-averaged moisture $q = q(x, y, t)$. In nondimensional units, the height of the tropopause is $H_T = \pi$ and the vertical velocity is assumed to be zero at the surface and tropopause. The vertical structure is then given by $\Psi_u(z) = \cos(z)$ and $\Psi_T(z) = \Psi_w(z) = \sin(z)$. Thus, the first baroclinic vertical structure and conservation of mass imply that

$$w = -\nabla \cdot \mathbf{u},$$

where the horizontal gradient is $\nabla = (\partial_x, \partial_y)$ and (x, y, z) represent the zonal, meridional, and upward distances, respectively.

Note that there is no baroclinic advection term in (1), which is consistent with the model presented in FMP04. We neglect not only the barotropic–baroclinic interaction but also, because of the Galerkin truncation, the baroclinic–baroclinic interaction as well.

The variables are nondimensionalized using the following units: the internal gravity wave speed $c = 50\,\mathrm{m\,s^{-1}}$, the Coriolis parameter $\beta = 2.28 \times 10^{-11}\ \mathrm{m^{-1}\ s^{-1}}$, the typical equatorial length scale $L_E = \sqrt{c/\beta} \approx 1500$ km, and the equatorial time scale $T_E = L_E/c \approx 8.3$ h. The prescribed gross moisture stratification is denoted $\tilde{Q}$. In this formulation, as in Neelin and Held (1987), Emanuel et al. (1994), and Sobel and Bretherton (2003), the gross moist stratification determines the moist phase speed of the waves. This relationship is also supported by studies with both idealized (e.g., Frierson 2007) and comprehensive GCMs (e.g., Lin et al. 2008).

The friction dissipation is parameterized by relaxation of velocities to zero with $\kappa = (10\ \mathrm{days})^{-1}$. Evaporation is parameterized by a drag formulation with fixed wind speed:

$$E = \frac{q_s - q}{\tau_e},$$

where a typical value for the evaporative time scale is $\tau_e = 10$ days. The saturation mixing ratio at the surface is denoted q_s and can depend on the zonal and meridional direction. The parameterization for the radiative processes is a Newtonian cooling, that is, a relaxation to a specified radiative equilibrium profile over a certain damping time ($\tau_r = 10$ days):

$$R = \frac{T - \overline{T}}{\tau_r}.$$

The precipitation parameterization is based on the Betts and Miller (1986) formulation. In this model, convection is active when moisture exceeds a reference saturation profile and it is then relaxed to the saturation value over a certain time scale. In regions where moisture is below saturation, convection is inactive and the precipitation vanishes. Mathematically,

$$P = \begin{cases} \dfrac{q - \hat{q}}{\tau_c}, & \text{if} \quad q > \hat{q}; \\ 0, & \text{if} \quad q \le \hat{q}. \end{cases} \tag{2}$$

In this formulation, τ_c is the convective adjustment time and $\hat{q}$ is the moisture saturation profile and will be treated as a constant. In FMP04 it is shown that a saturation profile that is a linear function of the potential temperature—$\hat{q} = \hat{q}_0 + \alpha T$ in (1)—is analogous to the case in which $\hat{q}$ is constant.

The spatial domain is a channel around the equator. A dry region is defined as a region where precipitation is inactive ($q < \hat{q}$) whereas a moist region is defined as a region where precipitation is active ($q \ge \hat{q}$). Variables are periodic in the zonal direction and tend to zero at the meridional boundary.

In FMP04, solutions of (1), as well as its gradient formulation, are shown to be bounded; moreover, their estimates do not depend on the convective adjustment time τ_c. Because the inequality holds for any finite τ_c, the solutions will be bounded when $\tau_c \to 0$, in agreement with the results presented by Stechmann and Majda (2006). This asymptotic limit in our model corresponds to the strict quasi-equilibrium from Emanuel et al. (1994). Physically, it means that moisture is instantaneously relaxed toward the moisture saturation profile; that is, in regions where convection is active, moisture must satisfy $q = \hat{q}$. A remarkable simplification of the SQE assumption is that (1) decouples into two shallow water systems propagating at distinct gravity wave speeds. To obtain these equations, note that when $P > 0$ and in SQE

$$q = \hat{q} \Rightarrow \partial_t q = 0 \Rightarrow P = E - \tilde{Q}\nabla \cdot \mathbf{u}. \tag{3}$$

Substituting (3) into (1c) gives the following shallow water system:

$$\partial_t u - \partial_x T - yv = -\kappa u, \tag{4a}$$

$$\partial_t v - \partial_y T + yu = -\kappa v, \quad \text{and} \tag{4b}$$

$$\partial_t T - c_0^2(\nabla \cdot \mathbf{u}) = E - R, \tag{4c}$$

where

$$c_0 = \begin{cases} c_m, & \text{if} \quad q > \hat{q}; \\ c_d, & \text{if} \quad q \le \hat{q}. \end{cases}$$

The moist gravity wave speed is $c_m = \sqrt{1 - \tilde{Q}}$; the dry gravity wave speed is $c_d = 1$. In dimensional units they correspond to $c_m = \sim 15$ m s^{-1} and $c_d \sim 50$ m s^{-1}.

This model allows for the study of the evolution of the interface between dry and moist regions and its interactions with the large-scale circulation. The theory is simpler in one dimension (in a line above the equator) because there is no meridional wind component and the free boundary can be interpreted as a propagating shock along the equator (the precipitation front). The precipitation front theory is developed in FMP04 and Pauluis et al. (2008) where, assuming SQE, the interface displacement and the transfer of signals between the dry and moist regions are investigated. The theory is then extended to a finite convective adjustment time in Stechmann and Majda (2006), again in one space dimension. In two dimensions, the interface between precipitating and nonprecipitating regions is more complex because it is no longer a single location, as it is in the one-dimensional case.

3. Methodology

Here, the SQE modeling framework is applied to develop an extension of the precipitation front theory to the study of equatorial waves on a β plane propagating along a precipitating band parallel to the equator (the ITCZ). The leading-order solution consists of a stationary and zonally independent flow. In this problem, the width of the precipitating region is controlled by the saturation mixing ratio at the surface, which we choose to be

$$q_s(y; \sigma) = \sigma \exp(-\sigma^2 y^2),$$

where σ is the nondimensional control parameter. The background flow resulting from this forcing corresponds to a Hadley circulation and a precipitating band centered at the equator. The equations, properties, and an outline for the analytical solution for the background state are presented in the appendixes.

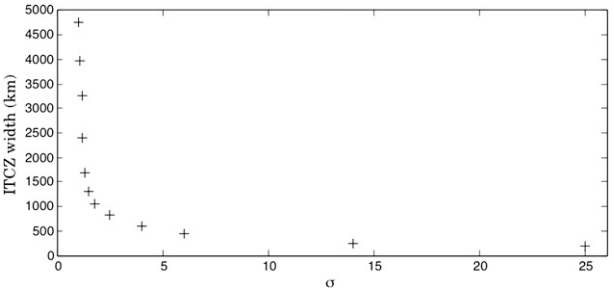

FIG. 1. Relationship between the ITCZ width and the variance (σ) of the forcing due to evaporation (q_s).

Figure 1 shows the relation between the parameter σ and the ITCZ width; in Fig. 2, the surface background flow for two distinct choices of σ is displayed. Because of the choice of q_s, the precipitating region is located at $(-y_0, y_0)$ and is surrounded by a region where precipitation is inactive, $(-\infty, -y_0)$ and (y_0, ∞), as can be seen in the bottom right of Fig. 2. The top panels show the Hadley circulation wind pattern at the surface and the bottom left panel shows that the potential temperature is higher nearby the equator.

In this model the idealized Hadley circulation is characterized by an inflow of air at the surface toward the precipitating region; because of the baroclinic structure, the flow moves toward the poles with the same amplitude at the top of the troposphere. The zonal wind amplitude is symmetric with respect to the equator with the maximum values in the subtropics, where the flow is westward at the surface and eastward at the tropopause with the same amplitude. The total imposed forcing is given by

$$Q_s = \int_{-\infty}^{\infty} q_s \, dy$$

and is kept constant; therefore, when the surface mixing ratio is concentrated close to the equator (larger σ), the meridional circulation is stronger than when the forcing is more spread (smaller σ), as Fig. 2 indicates.

For obvious reasons, the Hadley circulation in our highly idealized models differs in many ways from observation. For instance, the Galerkin formulation used here does not enforce angular momentum conservation, which is a key aspect of the Hadley circulation (Held and Hou 1980). However, for the purpose of this study, the only feature of the basic flow that impacts the CCEWs is the location and width of the precipitating

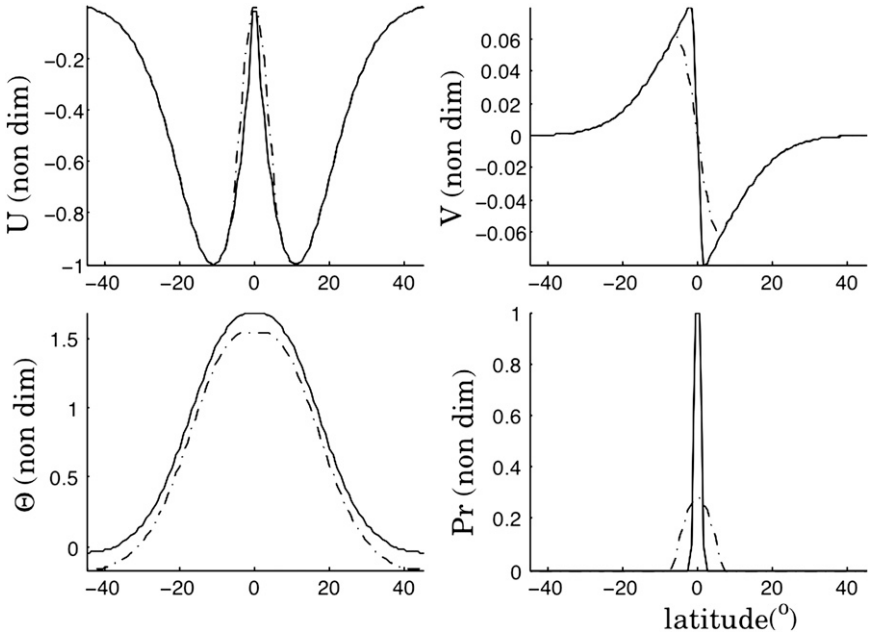

FIG. 2. Low-level stationary flow for $\sigma = 14$ (solid) and $\sigma = 6$ (dashed–dotted), normalized by their maximum value of the zonal wind; U is the zonal wind, V is the meridional wind, T is the potential temperature, and Pr is the precipitation rate.

region. Thus, the first baroclinic structure of the basic flow seems adequate.

To investigate the propagation of waves along the basic flow, the solution is decomposed as the sum of the steady zonally symmetric circulation and a small disturbance:

$$U(x,y,t) = \hat{U}(y) + \epsilon u(x,y,t), \tag{5a}$$

$$V(x,y,t) = \hat{V}(y) + \epsilon v(x,y,t), \tag{5b}$$

$$T(x,y,t) = \hat{T}(y) + \epsilon T(x,y,t), \quad \text{and} \tag{5c}$$

$$Q(x,y,t) = \hat{Q}(y) + \epsilon q(x,y,t). \tag{5d}$$

The solution to the basic flow (see appendixes) is stable for our choice of forcing q_s; therefore, this assumption is consistent with equations in (1) in which we assumed no barotropic wind. Moreover, because the system of Eqs. (4) is linear, there is no advection of the perturbation by the mean flow; that is

$$\partial_t u - \partial_x T - yv = 0, \tag{6a}$$

$$\partial_t v - \partial_y T + yu = 0, \quad \text{and} \tag{6b}$$

$$\partial_t T - c_0^2(\partial_x u + \partial_y v) = 0, \tag{6c}$$

where the gravity wave speed corresponds to

$$c_0 = \begin{cases} c_m, & \text{if} \quad |y| < y_0, \\ c_d, & \text{if} \quad |y| \geq y_0; \end{cases}$$

also, in Eq. (6) we neglected the terms on the rhs of (4) that only add linear damping to the solution and do not change the dynamics of the waves. The perturbation of moisture is determined by

$$q = \hat{q} \quad \text{if} \quad |y| < y_0, \quad \text{and} \tag{7}$$

$$\partial_t q + \tilde{Q}\nabla \cdot \mathbf{u} = 0 \quad \text{if} \quad |y| \geq y_0, \tag{8}$$

and the perturbation of precipitation is

$$P = -\tilde{Q}\nabla \cdot \mathbf{u} \quad \text{if} \quad |y| < y_0. \tag{9}$$

In FMP04 it is shown that smooth initial conditions for Eqs. (4) cannot develop discontinuities in u, v, T, and q in a single space dimension. In the appendixes we show that the interface between the precipitating and nonprecipitating regions must be continuous and the displacement of the interface has a second-order effect. As a result, in this formulation only the width of the ITCZ affects the disturbance equations and it is controlled exclusively by the parameter (from the forcing term) σ:

$$y_0 = y_0(\sigma).$$

The convectively coupled modes in this model are solutions of (6) when the ITCZ occupies a limited portion of the domain. That is, when the entire domain is dry ($y_0 = 0$) or moist ($y_0 = \infty$), solutions of the shallow water equations [(6a)–(6c)] are known and correspond to the modes obtained in Matsuno (1966) (e.g., Kelvin, Rossby, Yanai, and gravity waves); these are denoted here the free modes. Conversely, solutions in the presence of an interface between active and inactive precipitation regions—that is, when $y_0 \in (0, \infty)$—are the convectively coupled gravity waves. The convectively coupled modes are denoted according to their asymptotic limits when precipitation is active or inactive everywhere. For example, a convectively coupled Kelvin wave is a solution of Eq. (6) such that when $y_0 \to 0$ it approaches the dry Kelvin wave and when $y_0 \to \infty$ it approaches the moist Kelvin wave. Particularly, the CCEWs are solutions of the form

$$\Psi(x, y, t; y_0) = \sum_k \exp\{ik[x - c(k; y_0)t]\}\psi_k(y; y_0), \qquad (10)$$

where k is the zonal wavenumber and the speed of propagation must satisfy $C_m \le c \le C_d$ and the following asymptotic limits:

$$\sigma \to 0 \Rightarrow y_0(\sigma) \to \infty \Rightarrow c(k;\sigma) \to C_m(k), \text{ and} \qquad (11)$$

$$\sigma \to \infty \Rightarrow y_0(\sigma) \to 0 \Rightarrow c(k;\sigma) \to C_d(k), \qquad (12)$$

where C_m and C_d are the speed of the corresponding free moist and dry mode. In the subspace corresponding to convectively coupled Kelvin waves ($c_m k < \omega < c_d k$), we did not find any evidence of bifurcation at the parameter σ. However, it is possible that there are bifurcations in other regions of the spectrum.

In the traditional shallow water formulation from Matsuno (1966), equatorial trapped waves correspond to different modes of the form $\Phi = \exp[ik(x - \omega t)]\phi_n(y)$, where $(\phi_n)_0^\infty$ are the elements of the orthonormal parabolic cylinder basis and ω is the frequency ($c = \omega/k$). Although in this formulation the gravity wave speed is not constant, one can still look for a single plane wave solution of system (6) and therefore they can be combined into a single second-order ordinary differential equation (ODE) for the meridional velocity:

$$\psi_k''(y; y_0) + \left[\left(\frac{\omega^2}{c_0^2} - k^2 - \frac{k}{\omega}\right) - \frac{y^2}{c_0^2}\right]\psi_k(y; y_0) = 0, \qquad (13)$$

where $c_0 = c(y_0)$, ψ_k is the meridional amplitude of the wave, and

$$v_k(x, y, t) = \exp[i(kx - \omega t)]\psi_k(y; y_0).$$

The solution for a fixed $y_0 \in (0,\infty)$ is derived in the following manner: First, the two linear independent solutions in each region ($|y| < y_0$ and $|y| \ge y_0$) are obtained. Second, they must satisfy two constraints: solutions must vanish at infinity and must obey the matching condition at the interface that requires variables (u, v, T) to be continuous. Utilizing these two constrains, the complete solution is obtained; that is, the dispersion relation $\omega = \omega(k; y_0)$ and the meridional amplitude of the waves are determined. For a detailed derivation and discussion of the analytical solutions in SQE, see the appendixes.

Figure 3 shows the analytical dispersion relation for antisymmetric solutions of (13), where for simplicity only two coupled modes are displayed. On the right side of the plot, the dispersion curve corresponds to convectively coupled Kelvin waves for two distinct ITCZ widths. When the ITCZ is wider, the curve is closer to the moist theoretical curve ($\omega = c_m k$), whereas for a narrower ITCZ, it lies closer to the dry theoretical curve ($\omega = c_d k$). Analogous results are found for Rossby $M = 1$ waves, displayed on the left side of the plot. These results are further discussed in the next section.

To validate these solutions, we compare them to numerical solutions that are obtained utilizing the nonoscillatory balanced scheme, introduced by Khouider and Majda (2005a,b). Their scheme solves the full equations in (1); thus, in the appendix we describe the method to obtain the CCEW along the ITCZ that corresponds to the analytical solution. Furthermore, to understand how the location of the ITCZ affects these modes, we utilize the numerical scheme to extend the theory of CCEW to the case in which the ITCZ is shifted to the Northern Hemisphere—that is, $q_s = \sigma \exp[-\sigma^2(y - a)^2]$, where a is the location of the ITCZ. We then obtain propagating modes along the off-equatorial ITCZ that are similar to the traditional equatorial modes.

4. Results

In this section the dynamical structure of some CCEWs are illustrated for various ITCZ widths and locations. First, the ITCZ is centered at the equator and a Kelvin wave disturbance propagating along a narrow ITCZ ($y_0 \sim 250$ km) is described. This case is then compared to a Kelvin wave along a wider ITCZ ($y_0 \sim 1000$ km). Wavenumbers 1 and 6 are tested and numerical and analytical solutions are discussed. Next, the Kelvin wave disturbance propagating along an ITCZ off the equator is compared to the symmetric ITCZ case. The section ends with a comparison between a Rossby

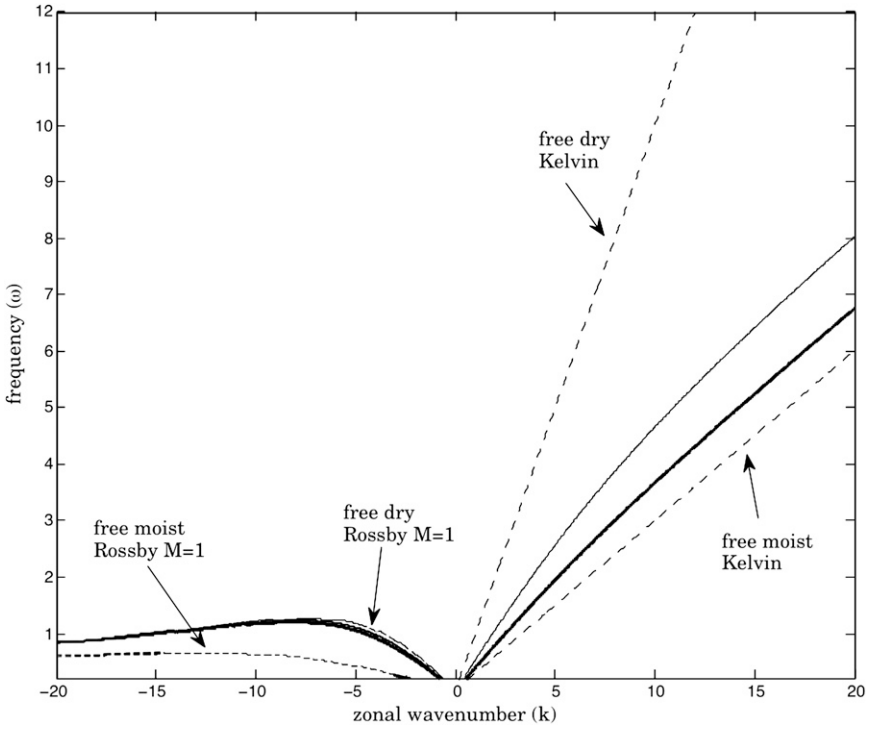

FIG. 3. Analytical dispersion relation for convectively coupled Kelvin and Rossby $M = 1$ waves, for $y_0 = 250$ km (thin lines) and $y_0 = 1000$ km (thick lines). The dashed lines correspond to the free dry and moist modes. The nondimensional zonal wavenumber is scaled by $1/L_E$ and nondimensional frequency is scaled by $1/T_E$.

wave $M = 1$ disturbance along a narrow and wide symmetric ITCZ.

a. Kelvin waves along a symmetric ITCZ

Many interesting features can be seen in the dispersion diagram in Fig. 3. The right-hand side (i.e., for positive wavenumbers) shows that the convectively coupled Kelvin waves propagate eastward and its phase speed ($c_p = \omega/k$) lies in the region $c_m < c_p < c_d$. The dispersion curve when $y_0 = 250$ km (thin line) is closer to the dry curve than with $y_0 = 1000$ km (thick line), as previously predicted. Remarkably, the convectively coupled Kelvin waves are only weakly dispersive; the dispersion curve is very close to a straight line in the frequency–wavenumber diagram.

Figure 4 shows a convectively coupled Kelvin wave for wavenumber 6 and $y_0 = 250$ km. The left (analytical) and right (numerical) panels indicate that the solutions are in close agreement. The zonal wind and potential temperature are both (top) in phase and then (bottom) out of phase with respect to the disturbance of the precipitation rate. The precipitation rate maximum occurs in the same region as the maximum wind convergence and the precipitation bandwidth and location remain unchanged. The structure of the potential temperature and zonal wind disturbance is similar to the free dry and moist modes (i.e., with opposite signs and a single maximum amplitude at the equator); however, they are not exactly proportional to each other, as they are for the free mode. Moreover, the meridional circulation is noticeable in this case, whereas for free modes, it is absent; in the next section we argue that these features are necessary to distribute the latent heat associated with the ITCZ.

In Fig. 5 we plot the phase speed of the Kelvin mode with respect to the ITCZ width for wavenumbers 1 and 6. In agreement with Fig. 3, the disturbance propagates faster for longer waves. Note that observed Kelvin waves (e.g., Wheeler and Kiladis 1999) show a similar faster propagation speed at smaller wavenumbers and also develop a meridional circulation (Wheeler et al. 2000, their Fig. 5). In the absence of the ITCZ, the mode propagates at the gravity wave speed (50 m s^{-1}). As the ITCZ becomes wider, the speed of the Kelvin coupled mode decreases; for an ITCZ width of about 1000 km, it propagates at the free moist speed (15 m s^{-1}). To further investigate the sensitivity of the dispersion relation to the ITCZ width, Fig. 6 shows the relation between the

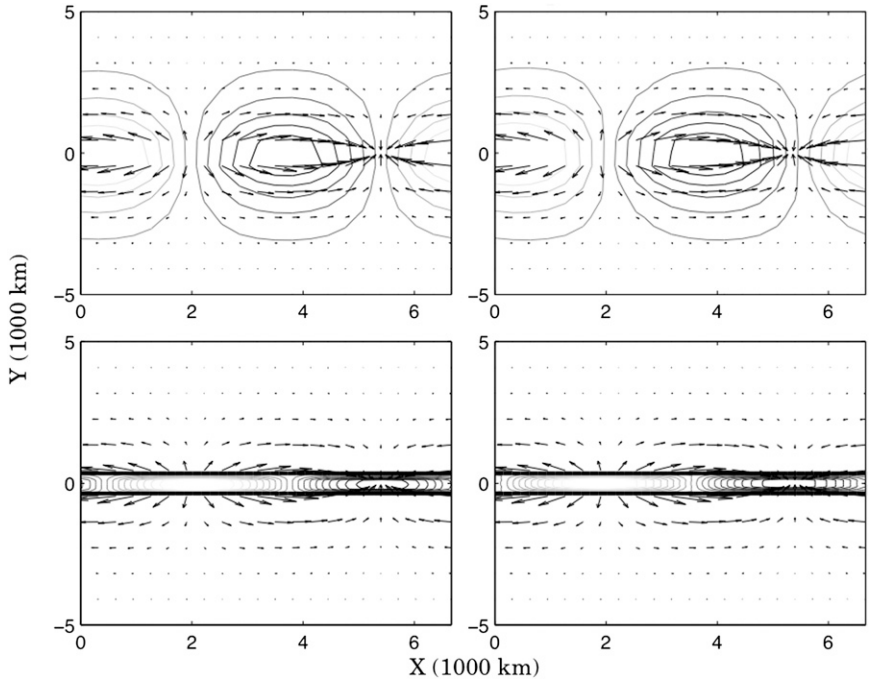

FIG. 4. Comparison between (left) analytical and (right) numerical solutions for a Kelvin wave ($k = 6$) with $y_0 = 250$ km (ITCZ centered at the equator). Overlaid are (top) a snapshot of contours of potential temperature and lower-level velocity profiles and (bottom) contours of the precipitation rate and lower-level velocity profiles. Dark contours correspond to negative values; the thick solid line corresponds to the ITCZ width. All variables are nondimensional.

ratio between the meridional flow and the zonal flow and the location of the interface, once more for wavenumbers 1 and 6. The ratio shown was computed using the analytical solution and we found a good agreement with the numerical result (not shown). For both wavelengths, the ratio is zero if there is no ITCZ (corresponding to the free dry Kelvin mode) and increases until the ITCZ width is about 400 km, when it starts to decrease with increasing ITCZ width. For narrower ITCZ widths, it is noticeable that the shorter wave ($k = 6$) develops a more intense meridional circulation. In the next section, we argue that the meridional wind increases with wavenumber.

b. *Kelvin waves along an ITCZ off the equator*

The analytical solutions used so far rely on the symmetry of the background state. Without this assumption, the disturbance response to the background state cannot be split into linear independent symmetric and antisymmetric components, as shown in the appendixes. We do not compute this analytical solution; instead, we show numerical results for the Kelvin wave disturbance propagating along a precipitating band off the equator (for details of this computation, see the appendixes). We test the same widths and wavenumbers from the last section, but now the ITCZ is centered at 10°N.

Figure 7 shows the potential temperature contour with the wind fields overlaid for a Kelvin wave $k = 1$ and ITCZ width $y_0 = 250$ km. The overall structure is similar to the case in which the ITCZ is centered at the equator; that is, the zonal wind and potential temperature are in phase (top plot), both are out of phase with respect to the disturbance of the precipitation rate (bottom plot), and its peak coincides with the maximum wind convergence zone. In agreement with Straub and Kiladis (2002, e.g., their Fig. 16), the inflow toward the precipitating region in regions of wind convergence is noticeable and, because the amplitude of the waves is very small at the northern interface, we observe a considerable stronger inflow at the southern interface. In Fig. 8 the amplitude of the disturbance is displayed for the Kelvin wave propagating along the symmetric ITCZ (dashed line) and along the off-equatorial ITCZ (solid line). Although no longer symmetric, the general structure of zonal wind and potential temperature meridional amplitude is fairly close to the ''free'' dry Kelvin wave and to the equatorial coupled mode. Importantly, these results suggest that the maximum precipitation rate (Fig. 8, bottom right) is smaller when the ITCZ is away from the equator; in the

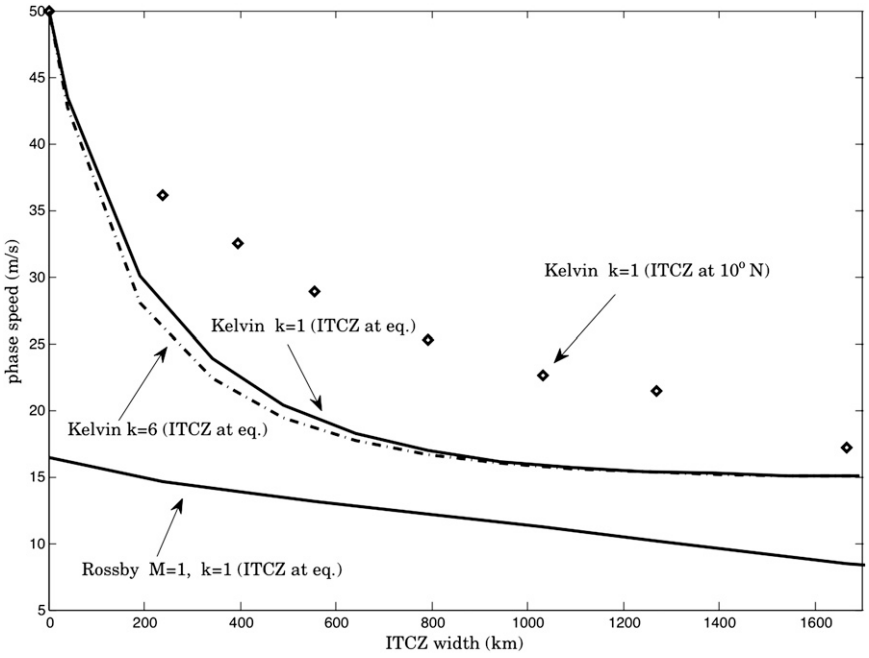

FIG. 5. Relationship between phase speed and ITCZ width for some of the coupled modes. The solid lines correspond to Kelvin and Rossby $M = 1$ modes along an ITCZ centered at the equator and wavenumber $k = 1$. The dotted–dashed line corresponds to a Kelvin mode along an ITCZ at the equator and wavenumber $k = 6$; the diamonds correspond to a Kelvin mode, $k = 1$, along an ITCZ centered at 10°N.

next section we argue that this is a consequence of the fact that the off-equatorial coupled mode propagates faster than the symmetric coupled mode for the same ITCZ width, as shown in Fig. 5. For instance, if the ITCZ width is $y_0 = 250$ km, the Kelvin mode when the ITCZ is centered at the equator propagates at about 28 m s^{-1}; in contrast, when the ITCZ is centered at 10°N, it propagates at about 35 m s^{-1}.

It is also worth noting that the meridional flow in Fig. 8 (right and left) has a sharp peak at the interface that indicates that the vertical velocity is discontinuous at the precipitation front, in agreement with the results from FMP04.

c. *Rossby wave M = 1 along a symmetric ITCZ*

Here we investigate the propagation of Rossby waves along a symmetric ITCZ. Analogous to the Kelvin wave experiment, the solution is known when $y_0 = 0$ and $y_0 = \infty$ because in both cases the equivalent depth is uniform in the whole domain and linear theory is valid. We examine the Rossby $M = 1$ mode, which propagates westward; it is dispersive and the zonal wind and potential temperature are symmetric across the equator. For small wavenumbers this mode propagates at about one third of the gravity wave speed; therefore, for long waves it determines the region in the dispersion diagram where we look for solutions: $-c_m k/3 < \omega < -k/3$.

Figure 9 is similar to Fig. 4, but for Rossby $M = 1$ and wavenumber $k = 1$. The analytical and numerical solutions are again in good agreement and the overall structure of this mode is similar to the free Rossby mode. Once more, potential temperature is out of phase with precipitation rate and convergence in the ITCZ is located at the peak of precipitation rate. However, wind also converges at higher latitudes, whereas for Kelvin waves it converges only at the ITCZ.

As can be seen on the left side of Fig. 3, the dispersion curve for the convectively coupled Rossby wave indeed lies between the dry and moist curves and exhibits a similar behavior to the free modes; that is, the dispersion relation is approximately linear for small wavenumbers and it decreases for large wavenumbers. However, the dispersion curves for both a narrow and a wide ITCZ are closer to the dry curve than for Kelvin waves, which indicates that Rossby waves are less affected by the ITCZ. Further evidence of this fact can be seen in Fig. 5, which shows a smoother and slower transition between the free dry and moist Rossby modes than the corresponding Kelvin mode (solid lines). That is, it is necessary to have a wider ITCZ to achieve the moist speed than for Kelvin waves. One explanation for this behavior is that because

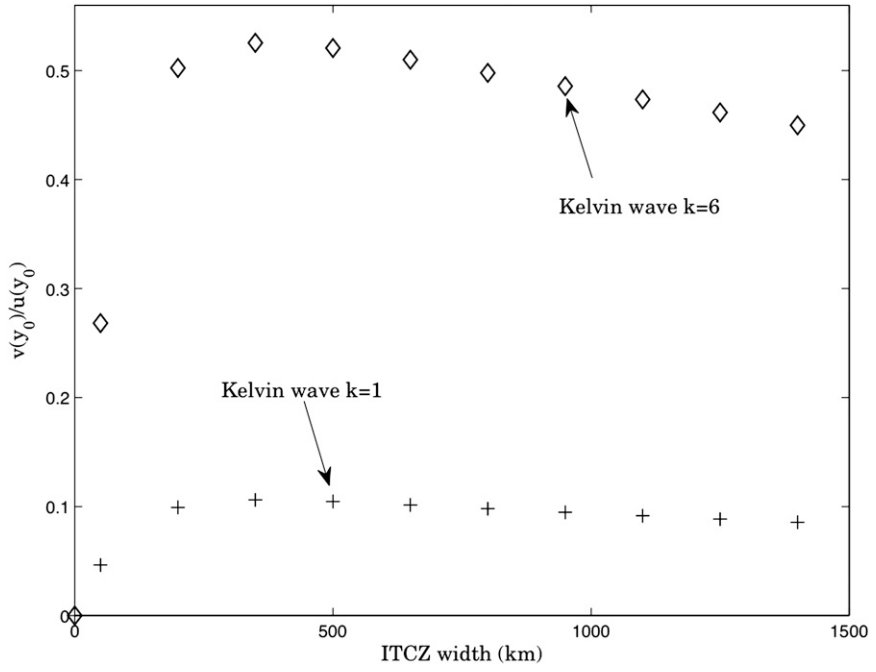

FIG. 6. Ratio between meridional and zonal wind at the interface $[|v(y_0)/u(y_0)|]$ for Kelvin wave $k = 1$ (crosses) and $k = 6$ (diamonds).

Rossby modes are strongly affected by the earth's rotation, the maximum convergence–divergence is located off the equator, in contrast to Kelvin waves.

5. Meridional circulation and modulations of the precipitation on the ITCZ

The propagation of convectively coupled waves along the ITCZ provides a useful framework to study the interactions between moist convection and the atmospheric dynamics. Here, we focus on some of the key aspects of the propagation of a Kelvin wave along the ITCZ. First, in contrast to the classic equatorial Kelvin wave on an equatorial beta plane, the Kelvin wave exhibits a meridional circulation. We argue that this circulation acts to redistribute the latent heat released in the ITCZ to the dry regions. This circulation modulates both the amount of precipitation and the width of the ITCZ itself, playing an important role in setting the propagation speed of the Kelvin wave.

a. The meridional circulation

In the previous section, convectively coupled Kelvin waves propagating along an ITCZ develop a meridional flow. This flow is stronger for short waves, but it is present even for long waves. Unlike most basic theoretical predictions, Kelvin wave composites in Wheeler et al. (2000) and Straub and Kiladis (2002) clearly show meridional velocities in both the upper and lower troposphere. To justify the existence of such meridional flow, let us focus on the equatorial ITCZ and suppose that the coupled modes satisfy $v = 0$. First, we compare the potential temperature tendency at the interface between the moist and dry regions in a region where the disturbance is associated with convergence at low level ($\partial_x u < 0$). In this case, we have

$$\partial_t T_d = \partial_x u < c_m^2 \partial_x u = \partial_t T_m. \tag{14}$$

The subscript m is used if $|y| < y_0$ and the subscript d if $|y| \geq y_0$ to denote the flow in the moist and dry regions, respectively. Because the flow is continuous, we must have $T_d = T_m$ at the interface. This also applies for the time tendency of the temperature. In particular, at the interface, we must have

$$\partial_t T_m(y_0) = \partial_t T_d(y_0). \tag{15}$$

However, in the absence of a meridional circulation $v = 0$, the inequality in (14) shows that ascending motion would cool the dry region faster than the moist region. Convectively coupled Kelvin waves must develop a meridional flow in order for the temperature tendencies to match at the edge of the ITCZ (15).

In regions where the atmosphere is cooling down, the flow at low levels must be into the ITCZ and toward the

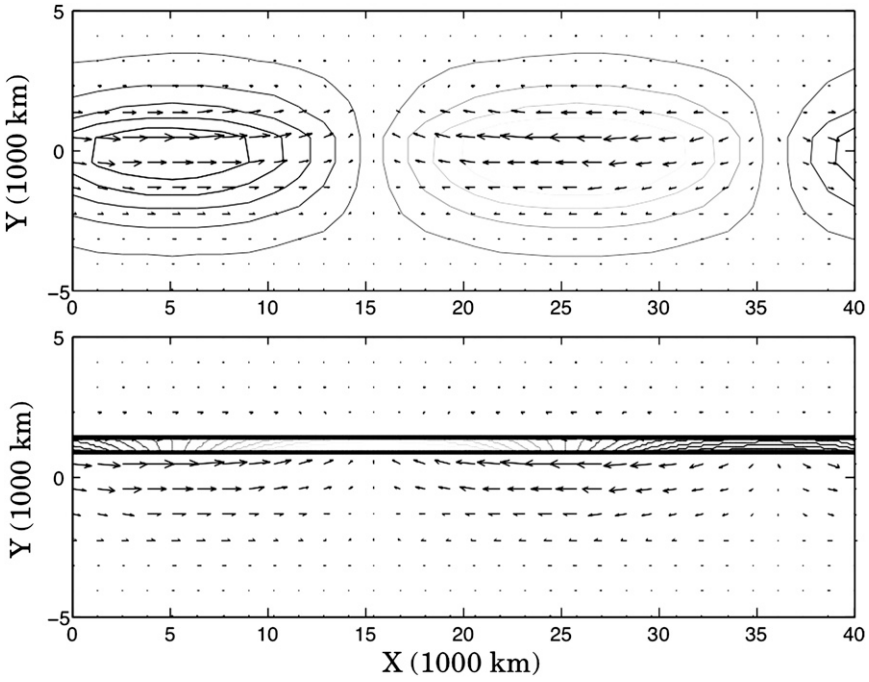

FIG. 7. Convectively coupled Kelvin wave ($k = 1$) along an ITCZ off the equator. Overlaid are (top) contours of potential temperature and velocity profiles and (bottom) contours of precipitation rate and velocity profiles. The ITCZ is centered at 10°N and $y_0 = 250$ km. Darker contours correspond to negative values. All variables are nondimensional.

equator. To assure that, we use (15) and subtract the potential temperature equation [(6c)] at the dry side of the interface from the same equation in the moist side:

$$\partial_y v^d - \partial_y v^m = -\frac{(1-c_m^2)}{c_m^2}\partial_t T. \tag{16}$$

We then estimate the meridional velocity at y_0:

$$\partial_y v^d \approx -\frac{v(t,x,y_0)}{L-y_0}, \quad \text{and} \tag{17a}$$

$$\partial_y v^m \approx \frac{v(t,x,y_0)}{y_0}, \tag{17b}$$

where L is the meridional extent of the Kelvin wave; and we used that $v(t, x, 0) = 0$. Combining (16) and (17), we obtain

$$\frac{(1-c_m^2)}{c_m^2}\partial_t T \approx \left(\frac{1}{L-y_0}+\frac{1}{y_0}\right)v(t,x,y_0). \tag{18}$$

Thus, when the atmosphere is cooling down ($\partial_t T < 0$), the meridional flow is toward the equator. A similar argument shows that

$$-\frac{v(t,x,y_0)}{L-y_0} - c_m^2\frac{v(t,x,y_0)}{y_0} \sim \partial_y v^d - c_m^2\partial_y v^m = -(1-c_m^2)\partial_x u.$$

Therefore, the meridional circulation associated with the convectively coupled Kelvin wave in regions of convergence is such that air flows toward the equator at the interface, rises in the area where precipitation is active, and then flows toward the poles at the tropopause, in agreement with Figs. 4 and 7. This meridional circulation cools the ITCZ by increasing the ascent and warms up the dry region.

b. The displacement of the interface

Because the zonal flow and potential temperature are continuous at the interface, there must be a discontinuity in the gradient of the meridional flow; accordingly, in the vertical velocity and from the temperature equation at the interface, we find that the discontinuity in the vertical velocity must satisfy

$$w^d(y_0) = c_m^2 w^m(y_0). \tag{19}$$

Hence, if at the edge of the moist region the flow is ascending, it has to be ascending at edge of the dry

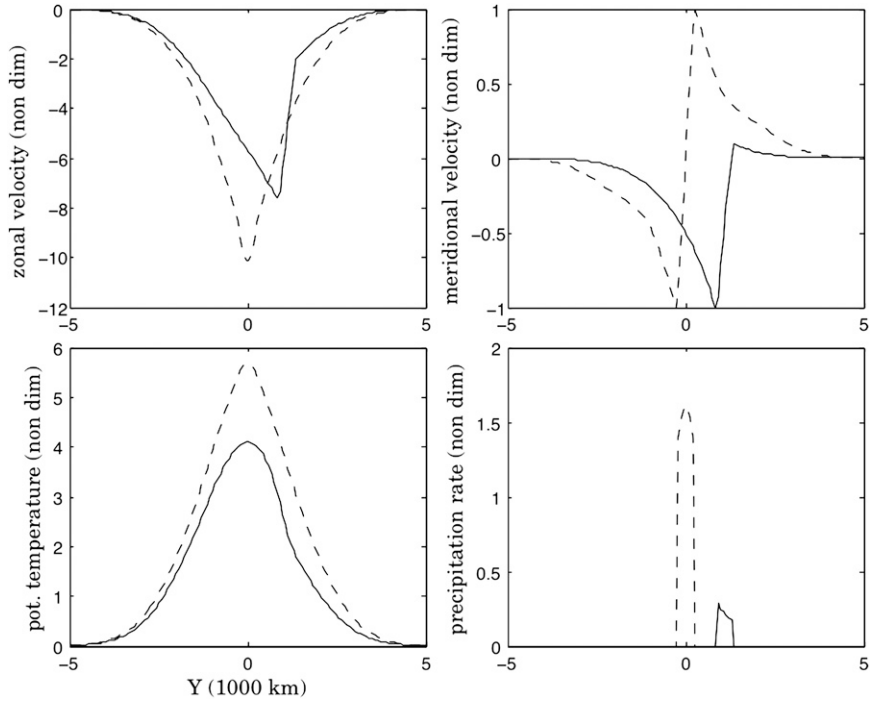

FIG. 8. Meridional structure for the convectively coupled Kelvin wave ($k = 1$) along the ITCZ centered at the equator (dashed line) and at 10°N (solid line), both with $y_0 = 250$ km. All variables are normalized by the maximum of the meridional velocity.

region, but its amplitude is reduced by c_m^2. In FMP04 the discontinuity in the vertical velocity at the interface is related to the propagation speed of the precipitation front, and we now argue that in regions of ascending motion, the interface moves toward the dry region, in agreement with FMP04.

The perturbation of moisture in a dry region satisfies

$$\partial_t q_d = \tilde{Q} w_d. \tag{20}$$

Thus, using the estimate for the interface displacement (A17) in regions of motion, we obtain

$$\partial_t \delta = \tilde{Q} \frac{w_d(x, y_0, t)}{|\partial_y Q_d(y_0)|} > 0 \quad \text{if} \quad y_0 > 0. \tag{21}$$

The ITCZ expands during the ascent phase of the Kelvin wave. Conversely, the ITCZ becomes narrower during the subsidence phase. It ensues that the variations of the ITCZ width by the Kelvin waves are out of phase by a quarter of a period with the variations of precipitation.

c. The speed of propagation

In section 4, we obtained a relation between the width of the ITCZ (y_0) and the speed of propagation of Kelvin and Rossby waves. Moreover, we found that this curve is in agreement with the numerical results. Because Kelvin waves have a simple structure, we focus our analysis on this mode. To better understand how the ITCZ affects this wave, it would be useful to relate its phase speed to the meridional circulation and the total precipitation rate in the ITCZ. To carry on this analysis, we average the equations in the meridional direction.

Here we assume that $u = \hat{U}(x - ct, y)$, $v = \hat{V}(x - ct, y)$, and $T = \hat{T}(x - ct, y)$, where c is the constant speed of propagation (from now on, we drop the hats). The meridional average is $\langle \phi \rangle = \int_{-\infty}^{\infty} \phi(y)\, dy$; the prime used below denotes the derivative with respect to the first variable. We also define the meridional average in the dry and moist region: $\langle \phi \rangle_d = \int_{-\infty}^{y_0} \phi(y)\, dy + \int_{y_0}^{\infty} \phi(y)\, dy$ and $\langle \phi \rangle_m = \int_{-y_0}^{y_0} \phi(y)\, dy$, respectively. Utilizing this notation, we define the parameter α as a measure of the ratio between the total latent heating and adiabatic cooling:

$$\alpha = -\frac{\langle P \rangle}{\langle U' \rangle}. \tag{22}$$

In the absence of precipitation $\alpha = 0$, whereas when precipitation is active everywhere $\alpha = \tilde{Q}$. To relate α to the phase speed of the Kelvin coupled wave, we compute the meridional average of (6):

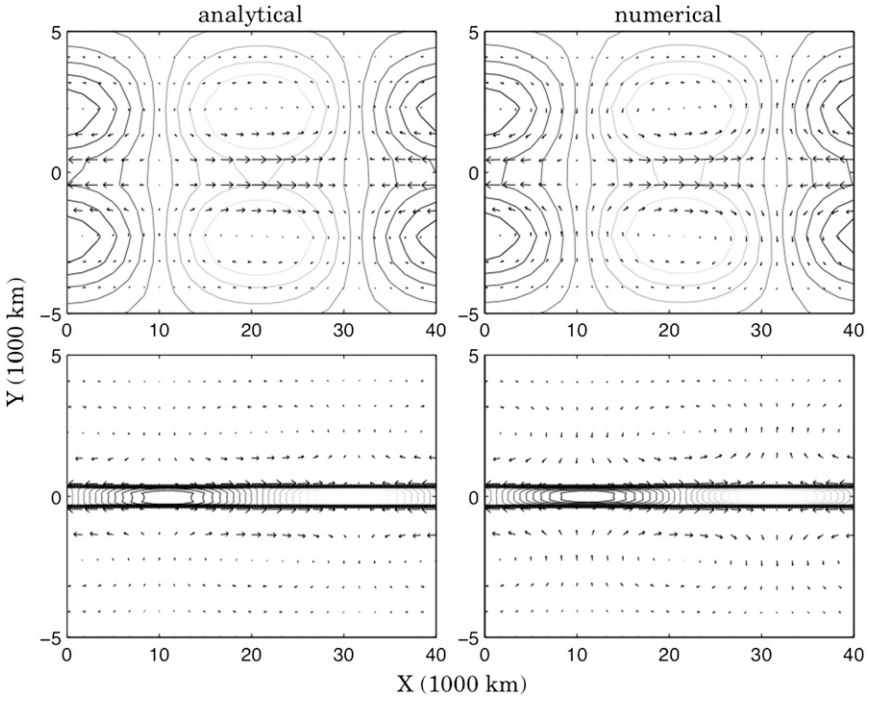

FIG. 9. As in Fig. 7, but for convectively coupled Rossby $M = 1$ wave ($k = 1$) along the ITCZ centered at the equator. The thick solid lines correspond to the ITCZ width.

$$-c\langle U'\rangle - \langle T'\rangle = \langle yV\rangle, \tag{23a}$$

$$-c\langle T'\rangle - c_d^2\langle U'\rangle = \langle P\rangle, \tag{23b}$$

where $\langle V\rangle = 0$ and $\langle V_y\rangle = 0$. Neglecting the rotation term on the right-hand side of (23a), the propagation speed becomes

$$c^2 = c_d^2 - \alpha. \tag{24}$$

The quantity $c_d^2 - \alpha$ can be thought as an equivalent to the effective stratification N_{eff}^2 in Emanuel et al. (1994) averaged over the meridional cross section of the Kelvin wave. The parameter α measures how much the latent heat release along a longitude circle slows down the coupled mode. Averaging (9), the mean precipitation is given by

$$\langle P\rangle = \langle P\rangle_m = -\tilde{Q}(\langle U'\rangle_m + \langle V_y\rangle_m). \tag{25}$$

Neglecting the meridional velocity and substituting (25) into (23b) yields an estimate for the propagation speed of the couple modes:

$$\phi(y) = \frac{-k}{\omega}\gamma(y) + i\frac{y}{\omega}\psi(y). \tag{26}$$

Moreover, if we look for a single propagating mode—that is, $U = U(y)e^{ik(x-ct)}$—the estimate above is equivalent to

$$c^2 = \frac{c_m^2\langle U\rangle_m + c_d^2\langle U\rangle_d}{\langle U\rangle_m + \langle U\rangle_d}. \tag{27}$$

If there is no meridional flow, the averaged coupled mode propagates at a speed that is the weighted average of the zonal wind amplitude in the moist and dry regions. In Fig. 10 this estimate is computed using the solution presented in the previous section. Comparing this estimate to the relation obtained in section 3 (Fig. 10), we find that although it has the correct limits when $y_0 \to 0$ and when $y_0 \to \infty$, the speed of propagation in (26) is considerable larger than the analytical speed of propagation.

We now compute an alternative estimate of the propagation speed that accounts for the meridional transport of temperature and moisture but neglects the Coriolis term yV in (23a). In this case, averaging the momentum equation over the moist regions yields

$$-c\langle U'\rangle_m - \langle T'\rangle_m = 0. \tag{28}$$

Similarly, averaging the temperature equation in the moist regions gives

$$-c\langle T'\rangle_m - c_d^2\langle U'\rangle_m - c_d^2\langle V_y\rangle_m = \langle P\rangle_m. \tag{29}$$

Using Eq. (25), we can now obtain an expression for the meridional velocity at the edge of the ITCZ:

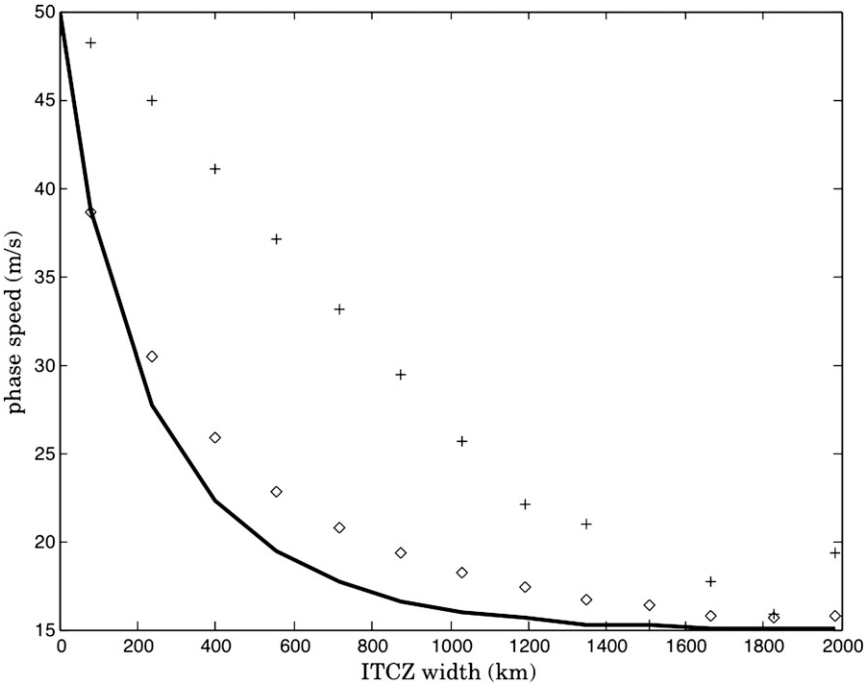

FIG. 10. Relationship between phase speed of the coupled Kelvin wave ($k = 1$) and the ITCZ width; comparison between the analytical phase speed (solid line) and the two approximations. The crosses correspond to the estimate in (26) and the diamonds to the estimate in (33).

$$2V(y_0) = \langle V_y \rangle_m = \frac{c^2 - c_m^2}{c_m^2} \langle U' \rangle_m. \tag{30}$$

The identity above relates the meridional flow to the average zonal flow and clarifies the balance between these quantities and the phase speed of the Kelvin mode. It is consistent with the estimate from the previous section in that it shows that if the zonal wind is convergent there is an inflow of air toward the ITCZ. In addition, for a single propagating mode, it is equivalent to

$$V(y_0) = \frac{1}{2} \frac{c^2 - c_m^2}{c_m^2} k \langle U \rangle_m \tag{31}$$

and indicates that the meridional flow is stronger for larger wavenumbers, in agreement with Fig. 6 and with observations.

Substituting (30) into (25) yields an expression for α:

$$\alpha = (c_d^2 - c_m^2) \frac{\langle U' \rangle_m + \langle V_y \rangle_m}{\langle U' \rangle} = c^2 \frac{c_d^2 - c_m^2}{c_m^2} \frac{\langle U' \rangle_m}{\langle U' \rangle}. \tag{32}$$

Injecting this in (24), we can obtain a new estimate for the propagation speed,

$$c^2 = \frac{\langle U' \rangle}{\dfrac{\langle U' \rangle_m}{c_m^2} + \dfrac{\langle U' \rangle_d}{c_d^2}} = \frac{\langle U \rangle}{\dfrac{\langle U \rangle_m}{c_m^2} + \dfrac{\langle U \rangle_d}{c_d^2}}, \tag{33}$$

and Fig. 10 shows that the second estimate (33) is considerable more accurate than the first one (26).

The precipitation is related to the total zonal wind convergence in the moist region using (32) and (22):

$$\langle P \rangle_m = -\frac{c^2}{c_m^2} \tilde{Q} \langle U' \rangle_m, \tag{34}$$

where the propagation speed c^2 in (33) is always larger than the moist speed c_m. This implies that the precipitation anomaly $\langle P \rangle_m$ is always larger than what one would infer based solely on the advection of moisture by the zonal wind. In sum, in regions of enhanced zonal wind convergence, the meridional flow advects moisture into the ITCZ, which increases the precipitation and slows down the propagation of the Kelvin wave.

6. Conclusions

We presented an extension to the SQE theory for convectively coupled gravity waves to cases in which the precipitating region only occupies a fraction of the

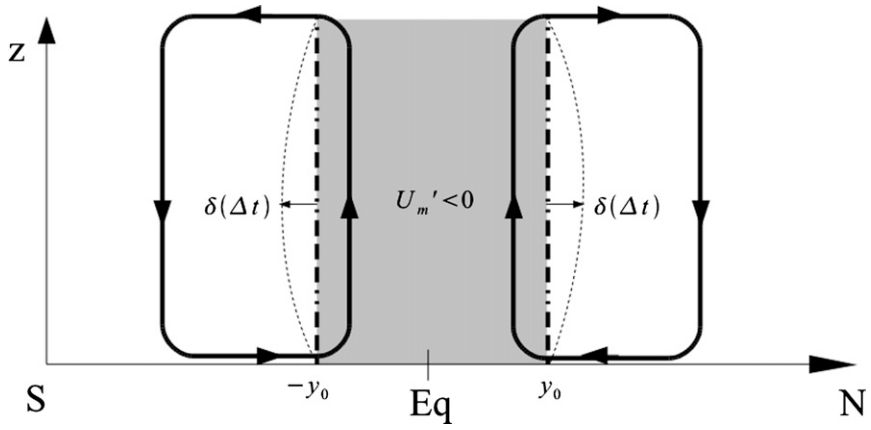

FIG. 11. Sketch of a cross section of the secondary circulation due to the ITCZ. The thick dotted–dashed vertical lines mark the two interfaces separating the dry regions and the moist (shaded) region; the thin dashed line represents the displacement of the interface. The arrows indicate the circulation pattern in a region where the zonal wind converges toward the equator.

domain. In particular, the conceptual simplification inherent in the SQE assumption leads us to build a simplified theory for CCEWs propagating over a precipitating band.

The key implication of the SQE within our model is that moisture is instantaneously adjusted to the saturation values in regions where precipitation is active; consequently, the problem was reduced to matching solutions of two shallow water systems, with distinct equivalent depths. Fundamentally, the matching comes from the requirement of the tendency in potential temperature to be continuous at the interface, and the discontinuity in the equivalent depth translates to a discontinuity in the vertical velocity.

This study is focused on convectively coupled Kelvin and Rossby waves propagating along the ITCZ, and we found that the propagation speed of the coupled waves is between the dry and moist speed, depending on the width and location of the precipitating band. Kelvin waves have speeds comparable to the moist case (15 m s^{-1}), except for narrow (less than 1000 km) precipitating regions; they propagate faster as the ITCZ moves away from the equator, they are weakly dispersive, and shorter waves propagate slower than long waves. The results also indicate that the ITCZ must be wider to have an impact on Rossby waves.

It has been shown that a meridional circulation, present even for Kelvin waves (Figs. 4, 6 and 8), plays an important role in redistributing energy between the dry and moist regions. At the surface and where the zonal wind converges, the meridional wind flows toward the ITCZ at the interface, ascends inside the precipitating region, and then flows toward the poles (Fig. 11). We proposed some interpretation of the mechanisms involved in this process by deriving a direct relationship among zonal wind convergence inside the ITCZ, total precipitation, and the speed of the coupled waves [(33) and (34)], which indicates that enhanced wind convergence is correlated with an increase in the precipitation rate and with the slowdown of waves.

In keeping with the secondary meridional circulation due to precipitation and in agreement with the theory of precipitation fronts presented in FMP04, we found that for temperature to match at the interface there must be a discontinuity in the vertical velocity that is proportional to the prescribed gross moisture stratification. Moreover, upward motions at the interface are related to the displacement of the ITCZ toward the poles; conversely, the interface moves toward the equator during the subsidence phase, as shown in Fig. 11.

Some key features of observed convectively coupled waves were well captured by the model: Kelvin waves propagate more slowly when convection is active; they are weakly dispersive and develop a meridional circulation. Because relatively few vertical modes seem to participate in many tropical phenomena involving the ensemble mean effects of deep convection, we believe that the extension of the method used here to other configurations (e.g., Rossby waves propagating over an off-equatorial ITCZ or a double ITCZ) can provide further insight into the coupling between convection and large-scale phenomena.

Acknowledgments. We thank Samuel Stechmann and Boualem Khouider for their help and advice regarding the numerical results. We also thank Paul Roundy, Dargan Frierson, Adam Sobel, and Zhiming Kuang for their careful and thoughtful suggestions to improve this paper.

APPENDIX A

Analytical Solutions for a Symmetric ITCZ

a. Stationary Hadley circulation

We use the assumptions from sections 2 and 3 to outline a stationary solution of (1) that depends only on the meridional distance. For simplicity, we also assume that $\tau_e = \tau_r = \kappa^{-1}$ and that $\hat{q} = 0$ and we then rewrite (4) as a single second-order ODE for each region. In the moist region we have

$$\left[\partial_{yy} - \frac{(\kappa^2 + y^2)}{c_m^2}\right]V = -\frac{\kappa}{c_m^2}\partial_y q_s, \quad \text{if} \quad P = \kappa\left(q_s - \frac{\tilde{Q}}{\kappa}\partial_y V\right) > 0. \quad \text{(A1)}$$

Similarly, in the dry region a solution of (4) must satisfy

$$[\partial_{yy} - (\kappa^2 + y^2)]V = 0, \quad \text{if} \quad Q = q_s - \frac{\tilde{Q}}{\kappa}\partial_y V \le 0. \quad \text{(A2)}$$

Equations (A1) and (A2) are known as the quantum harmonic oscillator and their solutions are expressed in terms of either parabolic cylinder equations—$D_\nu(y)[\nu = \nu(\kappa)]$, in which case there are two linear independent solutions, but only one of them vanishes at infinity (Bender and Orzag 1978)—or odd and even solutions related to the confluent hypergeometric function of the first kind (F_1^1) (Abramowitz and Stegun 1964). The forcing in (A1) is antisymmetric with respect to the equator and because we are interested in a stationary Hadley circulation solution, we seek a solution in which the meridional wind (V) points toward the equator. Therefore, in the moist region the solution is proportional to the odd linear independent solution, plus a particular solution due to the forcing term. In the dry region, we chose the solution that decays to zero for $y \to \infty$ and its odd extension for $y \to -\infty$.

It was shown in FMP04 that solutions of (4) have to obey some smooth properties. In particular, when the initial condition is smooth, solutions can only develop discontinuities due to planetary rotation; that is, the forcing term q_s can generate baroclinic instability. However, its development has a time scale much longer than the convective adjustment time, so in our formulation we choose q_s such that (U, V, T, Q) are continuous in the entire domain (including the interface). As a consequence, ($\partial_y V$, $\partial_y T$) are also continuous. Indeed, the following identities hold for $y < y_0$ and $y > y_0$:

$$\partial_y T = yU + \kappa V, \text{ and} \quad \text{(A3)}$$

$$\partial_y V = \frac{R - E}{c_m^2}. \quad \text{(A4)}$$

The interface is determined by $y_0 \in (0, \infty)$ such that

$$Q(y_0) = q_s(y_0) - \beta_1 \frac{\tilde{Q}}{\kappa}\partial_y V_d(y_0) = 0. \quad \text{(A5)}$$

This equation in SQE guarantees that Q is continuous at the interface. The variable β_1 is the free parameter that comes from the fact that the homogeneous solution of (A1) is well defined and unique up to a multiplicative constant. Similarly, in the moist region the full solution is $V_m(y) = \beta_2 V_m^h(y) + V_m^p(y)$, where β_2 is another free parameter. Therefore, we have three unknowns (y_0, β_1, β_2) and one equation [(A5)]. The two other equations come from the requirement that solution must be continuous:

$$\beta_1 V_d(y_0) = V_m(y_0), \text{ and} \quad \text{(A6)}$$

$$\beta_1 T_d(y_0) = T_m(y_0). \quad \text{(A7)}$$

We still have to show that in fact there will be a unique (β_1, β_2, y_0) that satisfy Eqs. (A5), (A6), and (A7). Because the dependence in β_1 and β_2 is linear, we can find a single equation only depending on y_0 that has the form $F(y_0, \sigma) = 0$ (recall that σ is fixed and comes from the forcing term), and then the width of the precipitating band is well defined as long as we can define $y_0 = f(\sigma)$ such that $F[\sigma, f(\sigma)] = 0$. The particular choice of q_s indicates that this is indeed the case. However, for simplicity, we obtain this solution numerically (it will be described later) and we verify that it satisfies the properties shown in this section.

b. Convectively coupled waves

Recall that we look for a plane wave solution of (6):

$$v_k(x, y, t) = \exp[i(kx - wt)]\psi_k(y; y_0), \quad \text{(A8a)}$$

$$v_k(x, y, t) = \exp[i(kx - wt)]\phi_k(y; y_0), \text{and} \quad \text{(A8b)}$$

$$T_k(x, y, t) = \exp[i(kx - wt)]\gamma_k(y; y_0). \quad \text{(A8c)}$$

Substituting (A8) into (6), we find that ψ_k solves the ODE in (13) and we obtain γ_k and ϕ_k using the following relations:

$$\gamma(y) = \frac{ic^2}{\omega^2 - c^2 k^2}[\omega\psi'(y) - ky\psi(y)], \quad \text{(A9)}$$

$$\phi(y) = \frac{-k}{\omega}\gamma(y) + i\frac{y}{\omega}\psi(y), \tag{A10}$$

where, for simplicity, we dropped the subscript k and the parameter y_0.

Note that (13) is, up to the coefficients, the same equation as (A2); likewise, the full solution can be decomposed into its symmetric and antisymmetric components. Particularly, the antisymmetric solution is

$$\psi_d(y) = D_{\nu-1/2}(\sqrt{2}y), \quad \text{and} \tag{A11}$$

$$\psi_m(y) = G^2(y/\epsilon_m), \tag{A12}$$

where

$$\nu = \frac{b_k}{2\sqrt{a}}, \quad \text{and}$$

$$\epsilon_m = \frac{\sqrt{c_m}}{2},$$

$$G_2(y) = ye^{-y^2}F_1^1\left(-\frac{\nu}{2} + \frac{3}{4}; \frac{3}{2}; \frac{y^2}{2}\right),$$

$$a = \frac{1}{c_0^2}, \quad \text{and} \quad b_k = \frac{\omega^2}{c_0^2} - k^2 - \frac{k}{\omega}.$$

The function $D_{\nu-1/2}$ is the parabolic cylinder function and it is chosen so that solutions decay at infinity. The function F_1^1 is the confluent hypergeometric function of the first kind and G_2 is an antisymmetric solution of (13). Recall that ν depends on c_0 and therefore it takes distinct values in the moist and dry region.

As in the Hadley circulation solution, the estimates from section (2) imply that the solutions must be continuous at the interface. Because the parameter ϵ is small, we assume that the interface will be a perturbation of the stationary interface from the background flow:

$$y = y_0 + \epsilon\delta(x,t), \tag{A13}$$

with matching conditions given by

$$\begin{aligned}
Q_d[y_0 + \epsilon\delta(x,t)] + \epsilon q_d[x, y_0 + \epsilon\delta(x,t), t] &= 0,\\
V_d[y_0 + \epsilon\delta(x,t)] + \epsilon v_d[x, y_0 + \epsilon\delta(x,t), t] &= V_m[y_0 + \epsilon\delta(x,t)] + \epsilon v_m[x, y_0 + \epsilon\delta(x,t), t], \quad \text{and}\\
T_d[y_0 + \epsilon\delta(x,t)] + \epsilon T_d[x, y_0 + \epsilon\delta(x,t), t] &= T_m[y_0 + \epsilon\delta(x,t)] + \epsilon T_m[x, y_0 + \epsilon\delta(x,t), t].
\end{aligned}$$

Next, we Taylor expand the above equations around y_0 and neglect the terms of $O(\epsilon^2)$:

$$\begin{aligned}
Q_d(y_0) + \epsilon\delta(x,t)\partial_y Q_d(y_0) + \epsilon q_d(x, y_0, t) &= 0,\\
V_d(y_0) + \epsilon\delta(x,t)\partial_y V_d(y_0) + \epsilon v_d(x, y_0, t) &= V_m(y_0) + \epsilon\delta(x,t)\partial_y V_m(y_0) + \epsilon v_m(x, y_0, t), \quad \text{and}\\
T_d(y_0) + \epsilon\delta(x,t)\partial_y T_d(y_0) + \epsilon T_d(x, y_0, t) &= T_m(y_0) + \epsilon\delta(x,t)\partial_y T_m(y_0) + \epsilon T_m(x, y_0, t).
\end{aligned}$$

and using the fact that V, T, Q, $\partial_y V(y)$ and $\partial_y T(y)$ are continuous, we obtain

$$\delta(x,t)\partial_y Q_d(y_0) + q_d(x, y_0, t) = 0s, \tag{A14}$$

$$v_d(x, y_0, t) = v_m(x, y_0, t), \quad \text{and} \tag{A15}$$

$$T_d(x, y_0, t) = T_m(x, y_0, t). \tag{A16}$$

Because Q_d is zero at the interface and negative for $y > y_0$, from (A14) we obtain an estimate of the displacement on the interface:

$$\delta(x,t) = \frac{q_d(x, y_0, t)}{|\partial_y Q_d(y_0)|}, \tag{A17}$$

where moisture is computed using (8). The matching conditions are given by (A15) and (A16), which are equivalent to

$$A(k,\omega) = \psi_m(y_0)\gamma_d(y_0) - \psi_d(y_0)\gamma_m(y_0) = 0, \tag{A18}$$

and we solve for $\omega(k; y_0)$; that is,

$$A[k, \omega(k; y_0)] = 0, \tag{A19}$$

where y_0 is fixed. There are several branches of solutions of (A19), each corresponding to a different convectively coupled mode. In Fig. 3, we show only the dispersion relation for the Kelvin and Rossby $M = 1$ coupled mode for two different values of y_0. Modes such as Rossby $M = 2$ and Yanai waves can be obtained computing the solution that corresponds to ψ symmetric with respect to the equator.

APPENDIX B

Numerical Solutions

Numerical solutions are obtained utilizing the nonoscillatory balanced scheme introduced by Khouider

and Majda (2005a,b). The convective adjustment time is set to 30 min so that numerical and analytical solutions can be compared. First, a family of stationary solutions is obtained by varying the parameter σ. The width of the ITCZ [$y_0 = y_0(\sigma)$] is then defined as the region parallel to the equator where precipitation is active. The basic flow solution corresponding to σ is given by

$$[U(y; \sigma), V(y; \sigma), T(y; \sigma), Q(y; \sigma), P(y; \sigma)].$$

For each fixed mean state, we need to obtain the CCEW solution. We first choose σ such that precipitation is active everywhere; that is, $y_0(\sigma)$ is of the size of the domain. In SQE, an asymptotic solution of the governing equations is given by a mode solution of (6); hence, we integrate the model with the initial condition given by the means state superimposed to an analytical solution of (6), where $c = c_m$ everywhere in the domain. Then, we average the disturbance along the path: $(x - c_m t = 0)$. To obtain a continuous spectrum of modes between the free dry and free moist solution, the parameter σ is then incremented in such a way that precipitation is active in almost the entire domain. The model is integrated with the new initial condition given by the mean state corresponding to the incremented σ, superimposed to the filtered disturbance.

At this point the speed of propagation of the strongest signal of the disturbance needs to be estimated; next, to filter out any signal that propagates at a different speed, the data are averaged along the path: $(x - c(\sigma)t = 0)$. This process needs to be repeated a few times until the disturbance corresponds to a single propagating mode with a speed given by $c(\sigma)$. In addition, at each iteration the disturbance is amplified by $e^{\kappa t}$ because the modes decay at the reciprocal of this rate due to linear damping.

Because the solutions are continuous as long as the increment of the ITCZ width is small compared to the size of the domain, the transition between the disturbance in one equilibrium state to the next one is smooth. Thus, we successively increase σ and repeat the method described above until the ITCZ width is close to zero. In the limit $y_0 \to 0$, the disturbance must converge to the free dry mode; that is, $c(\sigma) \to c_d$. As a result, for each σ, a solution of the form (10) is obtained.

To understand how the location of the ITCZ affects these modes, the location of the ITCZ can be shifted to the Northern Hemisphere. This is done by adding a new parameter to the saturation mixing ratio at the surface—$q_s = \sigma\exp[-\sigma^2(y - a)^2]$—and the result is a solutions of the form

$$\Psi(x, y, t) = A[x - c(\sigma, a)t]\psi(y; \sigma, a), \quad \text{(A20)}$$

where the case $a = 0$ corresponds to the ITCZ centered at the equator.

The transition between the ITCZ centered at the equator to one centered at a higher latitude is done in small steps and σ is fixed; hence, the propagating mode obtained for the new ITCZ location is denoted by the original mode corresponding to the ITCZ centered at the equator. That is, if one begins with a convectively coupled Kelvin wave disturbance along an ITCZ centered at the equator of width $y_0(\sigma)$, the mode obtained after shifting the ITCZ to a higher latitude is also denoted a convectively coupled Kelvin wave. In fact, it was numerically verified that these modes converge to the corresponding free dry mode when $y_0 \to 0$.

REFERENCES

Abramowitz, M., and I. A. Stegun, 1964: *Handbook of Mathematical Functions with Formulas, Graphs, and Mathematical Tables.* Dover, 1046 pp.

Arakawa, A., and W. H. Schubert, 1974: Interaction of a cumulus cloud ensemble with the large-scale environment, Part I. *J. Atmos. Sci.,* **31,** 674–701.

Bender, C., and S. Orzag, 1978: *Advanced Mathematical Methods for Scientists and Engineers.* McGraw-Hill, 593 pp.

Betts, A. K., 1986: A new convective adjustment scheme. Part I: Observational and theoretical basis. *Quart. J. Roy. Meteor. Soc.,* **112,** 677–691.

——, and M. J. Miller, 1986: A new convective adjustment scheme. Part II: Single column tests using GATE wave, BOMEX, ATEX and arctic air-mass data sets. *Quart. J. Roy. Meteor. Soc.,* **112,** 693–709.

Emanuel, K. A., 1986: Some dynamical aspects of precipitating convection. *J. Atmos. Sci.,* **43,** 2183–2198.

——, J. D. Neelin, and C. S. Bretherton, 1994: On large-scale circulations in convecting atmospheres. *Quart. J. Roy. Meteor. Soc.,* **120,** 1111–1143.

Frierson, D. M. W., 2007: Convectively coupled Kelvin waves in an idealized moist general circulation model. *J. Atmos. Sci.,* **64,** 2076–2090.

——, A. Majda, and O. Pauluis, 2004: Large scale dynamics of precipitation fronts in the tropical atmosphere: A novel relaxation limit. *Commun. Math. Sci.,* **2,** 591–626.

Gill, A. E., 1980: Some simple solutions for heat-induced tropical circulation. *Quart. J. Roy. Meteor. Soc.,* **106,** 447–462.

Held, I. M., and A. Y. Hou, 1980: Nonlinear axially symmetric circulations in a nearly inviscid atmosphere. *J. Atmos. Sci.,* **37,** 515–533.

Khouider, B., and A. Majda, 2005a: A non-oscillatory balanced scheme for an idealized tropical climate model. Part I: Algorithm and validation. *Theor. Comput. Fluid Dyn.,* **19,** 331–354.

——, and ——, 2005b: A non-oscillatory balanced scheme for an idealized tropical climate model. Part II: Nonlinear coupling and moisture effects. *Theor. Comput. Fluid Dyn.,* **19,** 355–375.

Lin, J.-L., M.-I. Lee, D. Kim, I.-S. Kang, and D. M. W. Frierson, 2008: The impacts of convective parameterization and moisture triggering on AGCM-simulated convectively coupled equatorial waves. *J. Climate,* **21,** 883–909.

Madden, R. A., and P. R. Julian, 1971: Detection of a 40–50-day oscillation in the zonal wind in the tropical Pacific. *J. Atmos. Sci.,* **28,** 702–708.

Matsuno, T., 1966: Quasi-geostrophic motions in the equatorial area. *J. Meteor. Soc. Japan,* **44,** 25–43.

Neelin, J. D., and I. M. Held, 1987: Modeling tropical convergence based on the moist static energy budget. *Mon. Wea. Rev.,* **115,** 3–12.

——, and N. Zeng, 2000: A quasi-equilibrium tropical circulation model—Formulation. *J. Atmos. Sci.,* **57,** 1741–1766.

Pauluis, O., 2004: Boundary layer dynamics and cross-equatorial Hadley circulation. *J. Atmos. Sci.,* **61,** 1161–1173.

——, A. Majda, and D. M. Frierson, 2008: Propagation, reflection and transmission of precipitation fronts in the tropical atmosphere. *Quart. J. Roy. Meteor. Soc.,* **134,** 913–930.

Sobel, A. H., and C. S. Bretherton, 2003: Large-scale waves interacting with deep convection in idealized mesoscale model simulations. *Tellus,* **55A,** 45–60.

Stechmann, S., and A. Majda, 2006: The structure of precipitation fronts for finite relaxation time. *Theor. Comput. Fluid Dyn.,* **20,** 377–404.

Straub, K. H., and G. N. Kiladis, 2002: Observations of a convectively coupled Kelvin wave in the eastern Pacific ITCZ. *J. Atmos. Sci.,* **59,** 30–53.

Takayabu, Y. N., 1994: Large-scale cloud disturbances associated with equatorial waves. Part I: Spectral features of the cloud disturbances. *J. Meteor. Soc. Japan,* **72,** 433–449.

Wheeler, M., and G. N. Kiladis, 1999: Convectively coupled equatorial waves: Analysis of clouds and temperature in the wavenumber–frequency domain. *J. Atmos. Sci.,* **56,** 374–399.

——, ——, and P. J. Webster, 2000: Large-scale dynamical fields associated with convectively coupled equatorial waves. *J. Atmos. Sci.,* **57,** 613–640.